JANUARY-1995 CB-NOTE 269

Technical report of the $\bar{p}d \rightarrow 2$ mesons + n analysis

Ulrike Thoma

Institut für Strahlen– und Kernphysik, Universität Bonn, D–53115 Bonn, Germany

Chapter 1

Preselection

The data for the analysis of the two mesons + neutron final states in liquid deuterium were taken from two run periods in May and October 1991.
Several preselection cuts ensure a rather clean data-set of 4 PED-events.

- events with residual charged events were rejected,
- exactly 4 PEDs ($E_{PED} \geq 20\,\mathrm{MeV}$) were required,
- events with PEDs in crystal type #13 were excluded.

Table 1.1 gives an overview of the data reduction for the zero-prong triggered data.

run period	May 1991	Oct. 1991	total
zero-prong-events	2651644	2211387	4863031
neutral events	2207957	2020488	4228445
events with 4 PEDs	122876	119392	242268
cut on type #13	111210	104976	216186
4 PED-events	111210	104976	216186

Table 1.1: *The result of the preselection using the zero–prong triggered data.*

Next a cut on the missing mass of the event was applied:

$$-150\,\mathrm{MeV}/c^2 \leq M_{miss} - M_{neutron} \leq +150\,\mathrm{MeV}/c^2 \tag{1.1}$$

Figure 1.1 shows the effect of this cut in an E_{tot} versus p_{tot} - plot.

The dataset is reduced to 100424 events, which were submit to kinematic fits. The corresponding two-photon invariant masses are shown in Figure 1.3.

These events were fitted kinematically.

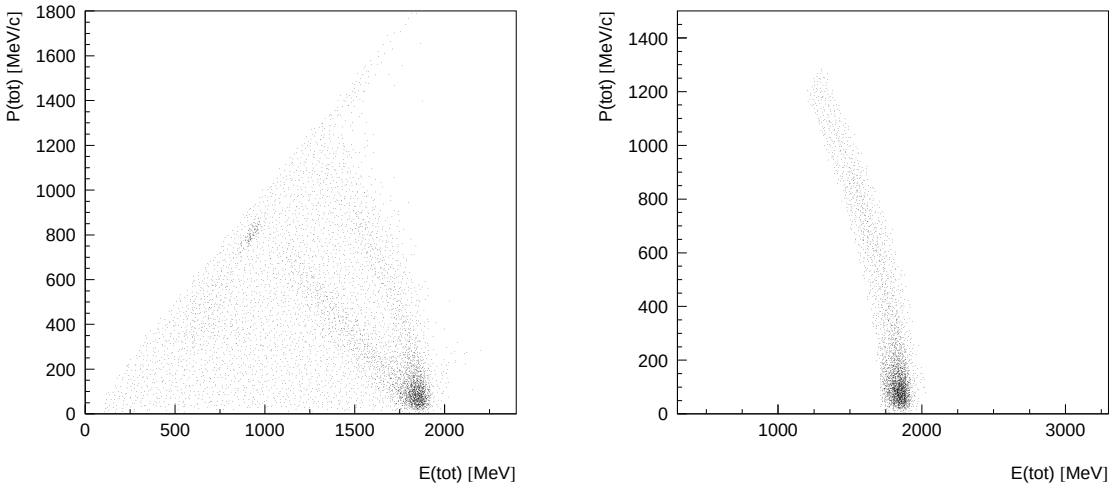

Figure 1.1: *Momentum versus energy (4 PED events): without (left) and with cut (right) on missing mass*

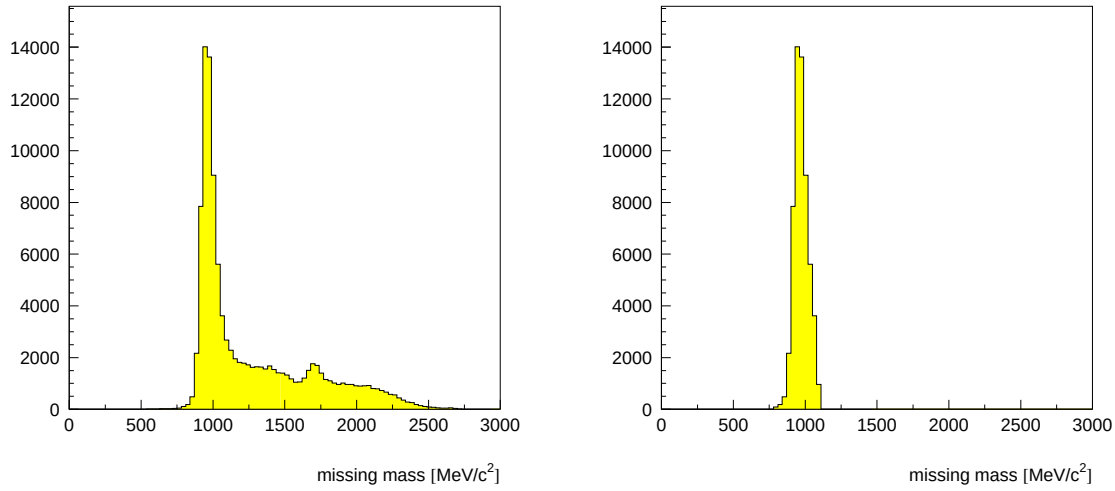

Figure 1.2: *Missing mass: without cut (left), with cut (right)*

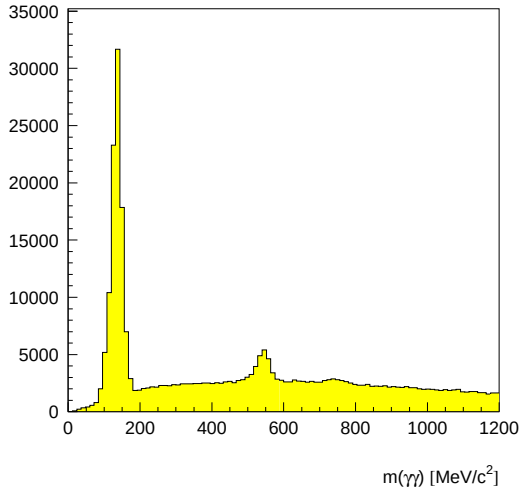

Figure 1.3: *Invariant photon-photon masses of the preselected events*

Chapter 2

Kinematic fitting

For the kinematic fit the standard program CBKFIT was used. The following hypotheses were tested:

$$\begin{array}{lcll} \bar{\mathrm{p}}\mathrm{d} & \rightarrow & 4\gamma + n & (1\mathrm{C}) \\ \bar{\mathrm{p}}\mathrm{d} & \rightarrow & \pi^0\pi^0 + n & (3\mathrm{C}) \\ \bar{\mathrm{p}}\mathrm{d} & \rightarrow & \pi^0\eta + n & (3\mathrm{C}) \\ \bar{\mathrm{p}}\mathrm{d} & \rightarrow & \eta\eta + n & (3\mathrm{C}) \\ \bar{\mathrm{p}}\mathrm{d} & \rightarrow & \pi^0\eta' + n & (3\mathrm{C}) \\ \bar{\mathrm{p}}\mathrm{d} & \rightarrow & \eta\eta' + n & (3\mathrm{C}) \end{array} \tag{2.1}$$

with each meson decaying into two photons:

$$\pi^0 \rightarrow \gamma\gamma, \quad \eta \rightarrow \gamma\gamma, \quad \eta' \rightarrow \gamma\gamma \tag{2.2}$$

Due to the combinatoric freedom of the 4γ final state one event can fit more than one hypothesis at once. Therefore an event is attributed to the hypothesis with the highest confidence level, where the confidence level is weighted by the relative branching ratio.

To achieve flat confidence level distributions and gaussian shaped pulls several error scalings were tried for the different run periods. In table 2.1 the scaling factors which were used are listed.

run period	energy	θ	ϕ
May 1991	0.027	1.26	1.26
October 1991	0.028	1.23	1.23

Table 2.1: *Correction factors for the kinematic fit*

Figure 2.1 shows the confidence level distribution for the hypothese $2\pi^0$+n and figure 2.2 shows the corresponding pulls for the three kinematic quantities. The gaussian function describes the distribution rather well with a standard deviation of ≈ 1 and a mean value of ≈ 0 except for $\sqrt{E}$. The exact values are given in table 2.2.

In table 2.3 the number of events fitting each hypotheses are given where a 1%-cut in the confidence level distribution of the 1C-Fit and a 10%-cut for the 3C-fits is applied.

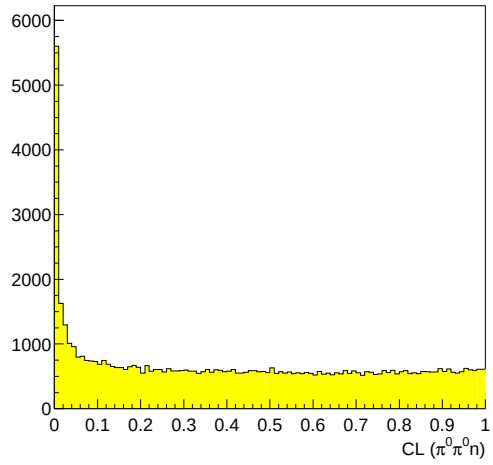

Figure 2.1:
Confidence level distribution for the hypothesis $2\pi^0$+n

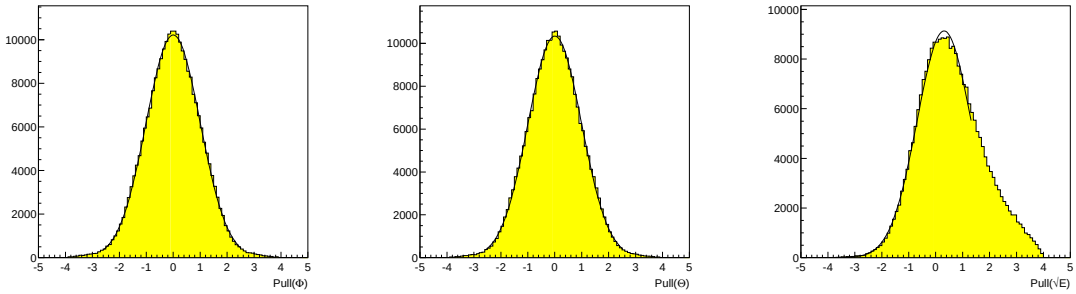

Figure 2.2: *Distribution of the pulls for the three kinematic quantities θ, ϕ and $\sqrt{E}$ for $\pi^0\pi^0 n$*

	$\bar{x}_\theta$	σ_θ	$\bar{x}_\phi$	σ_ϕ	$\bar{x}_{\sqrt{E}}$	$\sigma_{\sqrt{E}}$
$2\pi^0$+n	-0.001	1.0037	0.002	0.993	0.31	0.997

Table 2.2: *Mean and standard deviation of the pulls.*

hypothesis	#events
1C-Fit	86972
$2\pi^0$+n	52432
$\pi^0\eta$+n	7539
$\eta\eta$+n	1852
$\pi^0\eta'$+n	449
$\eta\eta'$+n	263

Table 2.3: *Result of the kinematic fit*

Figure 2.3a shows the $2\pi^0$+n-Dalitzplot. This plot is clearly dominated by events with low neutron momenta (see also figure 2.3b).

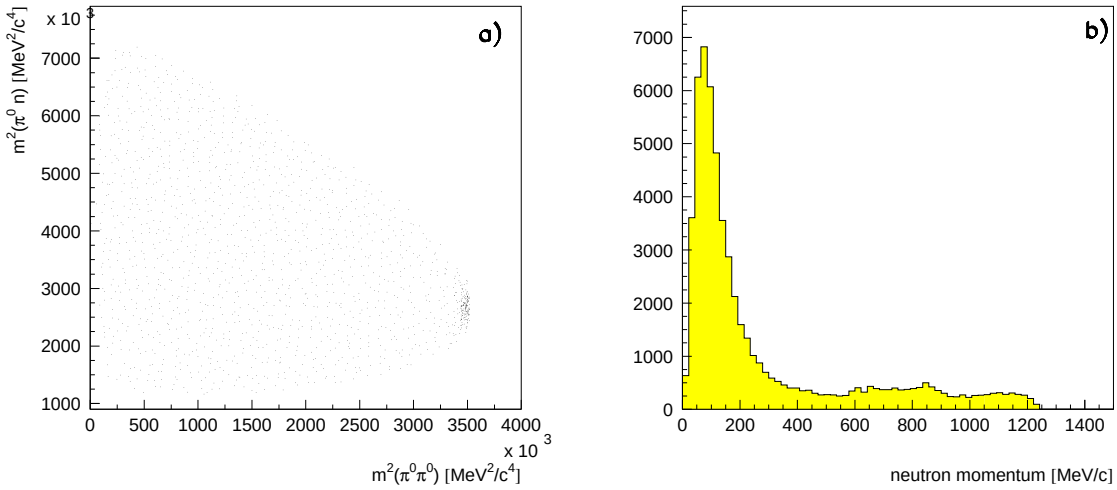

Figure 2.3: *$\pi^0\pi^0$+n-Dalitzplot and neutron momentum distribution (all neutral data)*

To be able to see any structures in the Dalitzplot the right part has been omitted (Figure 2.4).

The main feature of this Dalitzplot is a bandlike structure in the region of the $f_2(1270)$ and several structures in the direction of nucleon resonances. The nucleon resonance structure with the lowest mass can be identified with the $\Delta(1232)$, the next one is in the region of the N(1650) or $\Delta(1620)$ and the third enhancement corresponds to a mass of $\approx$ 1910 MeV. In order to analyse this Dalitzplot and to determine any branching ratio, it is necessary to consider some corrections. Further, possible background contributions have to be taken into account.

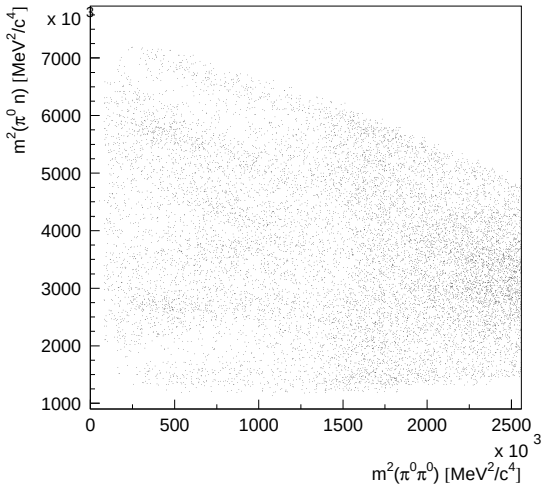

Figure 2.4:
$\pi^0\pi^0$+n-Dalitzplot with cut

Chapter 3

Monte-Carlo-studies

In order to give an estimate of the expected background contribution, Monte-Carlo simulations of some potential background channels were done. These were some 4γ-, 5γ- and 6γ-final states. A 5γ-event could contribute due to an undetected soft photon, a 6γ-event due to a lost meson. The reconstruction efficiencies for the $2\pi^0$+n- and $\pi^0\eta$+n-channels are also determined by Monte-Carlo simulations. The Monte-Carlo simulations for the background channels and for the determination of the global efficiencies were done by using the typical neutron momentum distribution for each channel to get the most realistic simulations. To explore whether the acceptance of the $2\pi^0$+n-channel has a flat distribution over the Dalitzplot a simulation of these events with a phase space distribution was done. The result is shown in figure 3.1

In table 3.1 the produced Monte-Carlo-events are listed.

generated final state	number of generated events
$\pi^0\pi^0$ +n	120000 (phase space distributed)
$\pi^0\eta$ +n	120000 (phase space distributed)
$\pi^0\pi^0$ +n	120000
$\pi^0\eta$ +n	120000
$\pi^0\pi^0\pi^0$+n	60000
$\pi^0\pi^0\eta$ +n	60000
$\pi^0\eta\eta$ +n	40000
$\pi^0\omega$ +n	40000

Table 3.1: *Overview of the generated Monte-Carlo-events*

The generated events passed the same analysis chain as real data. The expected background contribution for the $2\pi^0$+n- and $\pi^0\eta$+n-channels is given in table 3.2 and in table 3.3. It can only be a rough estimate because the branching ratios of the different channels are not exactly known. Table 3.4 shows the reconstruction efficiencies for the two channels.

The background to the $\pi^0\pi^0$ +n channel is estimated to be less than 1.5%.

generated final state	identified as $\pi^0\pi^0$+n reconstructed MC-events	true events	relative contribution
$\pi^0\eta + n$	5	0.82	$1.56 \cdot 10^{-5}$
$\pi^0\pi^0\pi^0$+n	7	88	$1.68 \cdot 10^{-3}$
$\pi^0\pi^0\eta + n$	0	0	0.0
$\pi^0\eta\eta + n$	0	0	0.0
$\pi^0\omega + n$	38	74.5	$1.42 \cdot 10^{-3}$

Table 3.2: *Expected background contribution to $\pi^0\pi^0$+n*

generated final state	identified as $\pi^0\eta$+n reconstructed MC-events	true events	relative contribution
$\pi^0\pi^0$+n	30	29.95	$3.97 \cdot 10^{-3}$
$\pi^0\pi^0\pi^0$+n	12	150.9	$2.0 \cdot 10^{-2}$
$\pi^0\pi^0\eta$+n	2	6.93	$9.2 \cdot 10^{-4}$
$\pi^0\eta\eta$+n	0	0	0.0
$\pi^0\omega$+n	34	66.67	$8.84 \cdot 10^{-3}$

Table 3.3: *Expected background contribution to $\pi^0\eta$+n*

	generated MC-events	reconstructed MC-events	global MC-efficiency (ε_{MC})
$\pi^0\pi^0 + n$	120000	55602	$0.46 \pm 2.38 \cdot 10^{-3}$
$\pi^0\eta + n$	120000	51785	$0.43 \pm 2.27 \cdot 10^{-3}$

Table 3.4: *Monte-Carlo-efficiencies (events produced with neutron momentum distribution)*

	generated MC-events	reconstructed MC-events	MC-efficiency (ε_{MC})
$\pi^0\pi^0 + n$ (whole DP)	120000	53105	$0.44 \pm 2.31 \cdot 10^{-3}$
$\pi^0\pi^0 + n$ (π^0 backward emission)	60000	25891	$0.43 \pm 3.20 \cdot 10^{-3}$

Table 3.5: *Monte-Carlo-efficiencies (events produced with phase space distribution)*

Most of the background events are in the region with low neutron momentum ($\leq$ 350 MeV), as expected because of the neutron momentum distribution. Therefore they have no influence on the determination of the $\Delta(1232)$-branching ratio.

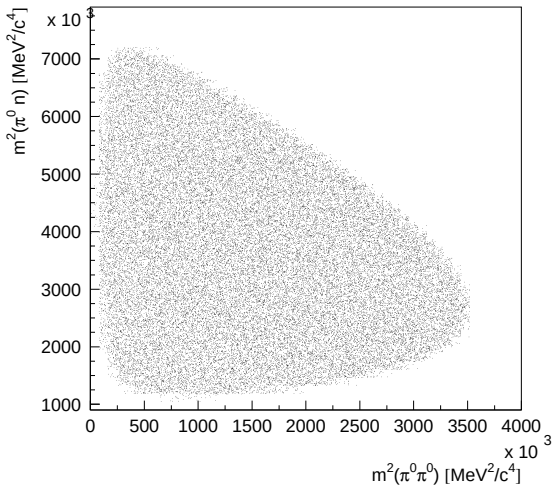

Figure 3.1:
$2\pi^0$+n Dalitz plot from Monte-Carlo events (phase space simulation)

Figure 3.1 shows that the distribution of the Monte-Carlo-events over the Dalitzplot is flat ($\pm$ 2%), this means that there are no structures in the Dalitzplot. But the detection efficiency for π^0 backward emission is about $\approx$ 1% lower than the mean value for the whole Dalitzplot (Table 3.5). This value was used for the determination of the $\Delta(1232)$ branching ratio.

Chapter 4

The neutron detection efficiency

Up to this point only the four-PED-dataset was considered, but it is also possible that the neutron interacts in the barrel and produces an additional PED. So the four-PED-dataset has to be corrected for events which are lost due to the neutron interaction in the barrel.

It is not possible to determine the probability for the neutron not being detected only by Monte-Carlo-simulations. So it was necessary to use experimental informations to determine this probability. We used the reaction $\bar{p}d \rightarrow 3\pi^0 + n$ in both six- and seven-PED final state [2], a reaction with a relatively large branching ratio so that it yields a high statistics sample. As the final state consists of more than two particles, the neutron momentum varies over a wide range. Figure 4.1 presents (as a function of neutron momentum) the ratio (ε) of events observed in seven-PED, assuming the 7th PED is an neutron, to the sum of events in six- or seven PED data.

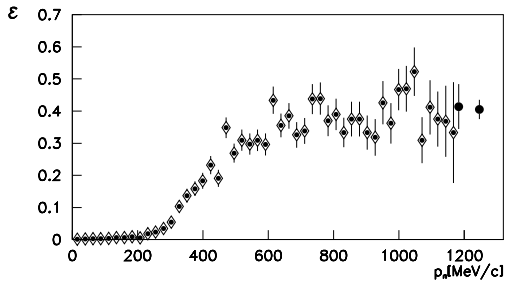

Figure 4.1:
Neutron detection efficiency

A parametrisation of this distribution is given in [2]. This parametrisation is used in the following analysis.
The efficiency for the neutron not being detected is now

$$\varepsilon_n \;=\; 1 \;-\; \varepsilon - 0.02 \;\;, \tag{4.1}$$

where the correction factor 0.02 is due to events where the the neutron produces more than one additional PED [2] this factor has only to be considered for high energy neutrons. The error of this efficiency was estimated to be 0.04 [1]

Chapter 5

Total number of annihilations

To determine the absolute number of annihilations, which corresponds to the zero-prong-dataset, minimum bias data from two runperiods May and Oct. 1991 were used. The mininmum bias dataset was analysed with the same cuts as the dataset taken with the zero-prong-trigger to get the $2\pi^0$+n-events for normalisation.

run period	May 1991	Oct. 1991	total
min.bias-events	1004932	852669	1857601
zero-prong-events	25548	23142	48690
4 PED-events	1310	1261	2571
$2\pi^0$ +n-events	221	226	447

Table 5.1: *Selection of $2\pi^0$+n-events from min.bias data*

The total number of annihilations was calculated by the following formula:

$$N(\bar{\mathrm{p}}\mathrm{d}\rightarrow all) = \frac{N^{0-prong}(2\pi^0+n)}{N^{min.bias}(2\pi^0+n)} \cdot N^{min.bias} \cdot \varepsilon \tag{5.1}$$

Where $N^{min.bias}$ is the number of antiprotons for the open trigger run and a correction factor of ε=0.956±0.025 for antiprotons lost due the interactions in the beam counters and material in front of the target. In this way we obtain the final number of annihilations that must have led to the observed number of $2\pi^0$+n-events:

$$N(\bar{\mathrm{p}}\mathrm{d}\rightarrow all) = (208.3 \pm 11.3) \cdot 10^6 \tag{5.2}$$

Chapter 6

$2\pi^0$+n- and $\pi^0\eta$+n-branching ratio

To determine the branching ratios, the data has to be corrected for the neutron- ($\varepsilon_{n.detec.} = 1 - \varepsilon$) and Monte-Carlo- ($\varepsilon_{MC}$) detection-efficiencies. In addition the branching ratios of the mesons decaying into two photons has to be taken into account ($\varepsilon_{meson \to \gamma\gamma}$).

$$BR(\bar{\mathrm{p}}\mathrm{d} \to 2mesons + n) = \frac{N^{0-prong}(2mesons + n)}{N^{min.bias} \cdot \varepsilon_{n.detec.} \cdot \varepsilon_{MC} \cdot \varepsilon_{meson1 \to \gamma\gamma} \cdot \varepsilon_{meson2 \to \gamma\gamma}} \tag{6.1}$$

Thus the following branching ratios are obtained:

$$BR(\bar{\mathrm{p}}\mathrm{d} \to 2\pi^0 + n) = (5.90 \pm 0.32) \cdot 10^{-4} \tag{6.2}$$

$$BR(\bar{\mathrm{p}}\mathrm{d} \to \pi^0\eta + n) = (2.46 \pm 0.12) \cdot 10^{-4} \tag{6.3}$$

Chapter 7

Branching ratio for the Pontecorvo reaction $\bar{p}d \rightarrow \Delta(1232) + \pi^0$

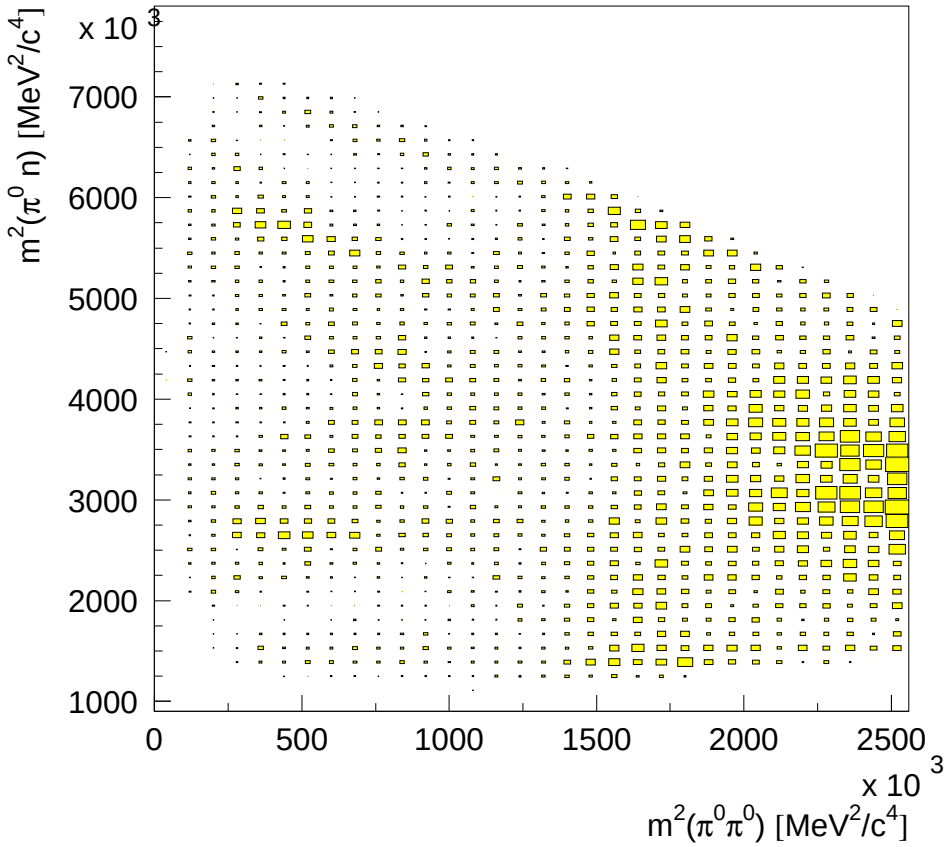

Figure 7.1: $\pi^0\pi^0$+*n-Dalitzplot*

The $\pi^0\pi^0 n$-Dalitzplot shows a clear bandlike structure in the region of the $\Delta(1232)$ invariant mass. The aim of this chapter is to explain how it is possible to determine the branching ratio of the $\Delta(1232)$ without fitting the Dalitzplot, which would be a very difficult task due to our unprecise knowledge of the neutron momentum distribution and the big interference effects of an unknown number of nucleon resonances.
Close to the $\Delta(1232)$ there are no other known nucleon resonances, so that it is possible to identify the bandlike structure with the $\Delta(1232)$, as the distribution along $\cos(\Theta)$, the decay angle of the resonance in the Gottfried-Jackson-system, is always symmetrical. If it is possible to determine the number of events along the half of the angular distribution one can multiply this number by two in order to get the total number of events. However before doing any analysis of angular distributions and their projections, one has the correct first on the neutron-detection-efficiency, which depends on the neutron momentum.

Figure 7.2 shows the corrected Dalitzplot (each event was weightend by $1/(1\text{-}\varepsilon)$ and the corresponding distribution versus the $\cos(\Theta)$.

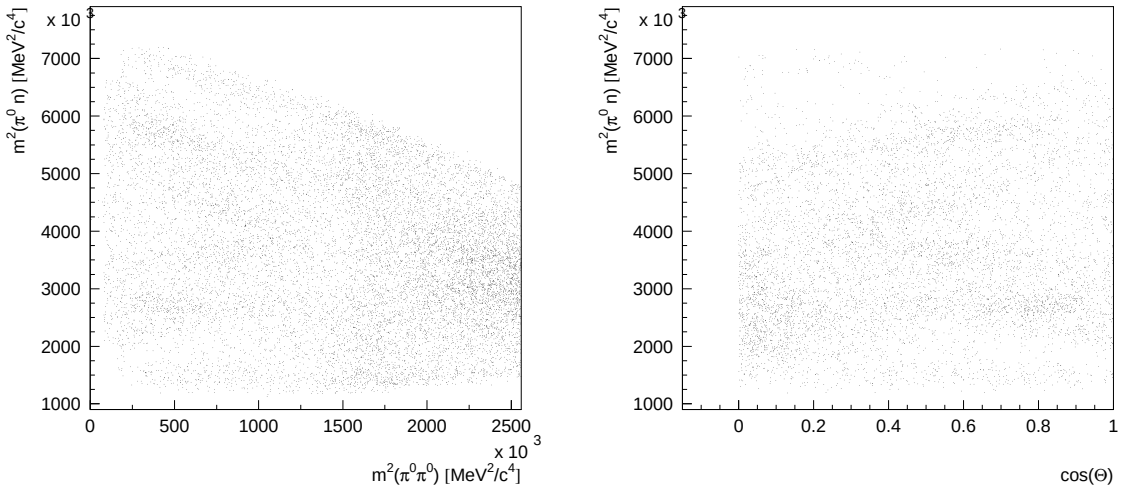

Figure 7.2: *Corrected Dalitzplot and distribution versus the cos(*Θ*).*

Figure 7.2 shows that for low $\pi^0\pi^0$-invariant masses, i.e. for $\cos(\Theta)$ values greater than 0.5 there are almost no events between the two nucleon resonance structures. This means that there should be no background in the $\Delta(1232)$ region too. The $\Delta(1232)$ band seems to be flat up to the point where the $f_2(1270)$ resonance structure crosses. To see in which parts of the angular distribution the $f_2(1270)$ causes an enhancement, Figure 7.3 shows the same plot with simulated $f_2(1270)$+n-events. To understand the structures of the invariant mass plot better and to show why there should be nearly no background in the $\Delta(1232)$ region, some more results from Monte-Carlo-simulations are shown at the end of this report.

Mass and width of the $\Delta(1232)$ are determined by using a projection on π^0 n invariant mass. Moreover a cut on the invariant $\pi^0\pi^0$-mass was applied in order to suppress the

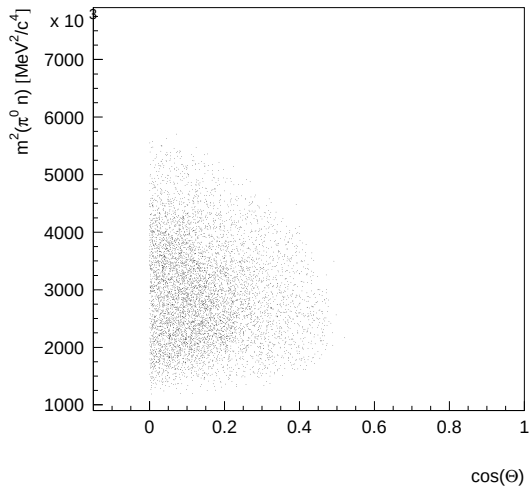

Figure 7.3:
$f_2(1270)$ distribution versus the $\cos(\Theta)$.

$f_2(1270)$ background ($m_{\pi^0\pi^0} \leq 1000$ MeV).

Figure 7.4 shows the $\pi^0 n$ invariant mass after this mass cut and the equivalent plot where the $\Delta(1232)$ is fitted by a Breit-Wigner amplitude which is weighted with the phase-space distribution determined by Monte-Carlo-simulations.

The fit results for three different cuts are listed in Table 7.1:

cut in inv. $\pi^0\pi^0$-mass	fitted mass	fitted width
1100 MeV/ c^2	1233.9 $\pm$4.06	129.16 $\pm$12.63
1000 MeV/ c^2	1230.6 $\pm$4.11	120.8 $\pm$12.84
900 MeV/ c^2	1228.0 $\pm$4.54	111.55 $\pm$12.95

Table 7.1: *Fit results for mass and width of the $\Delta(1232)$*

Because of the possible background from $f_2(1270)$, in case of a cut at 1100 MeV/ c^2 and due to the lack of statistics if a cut at 900 MeV/ c^2 is used, the 1000 MeV/ c^2-cut was taken to determine mass and width of the $\Delta(1232)$. The result

$$M_{\Delta(1232)} = (1230.6 \pm 4.1)\,\mathrm{MeV}/c^2 \tag{7.1}$$

$$\Gamma_{\Delta(1232)} = (120.8 \pm 12.8)\,\mathrm{MeV}/c^2 \tag{7.2}$$

is in good agreement with values given in [3].

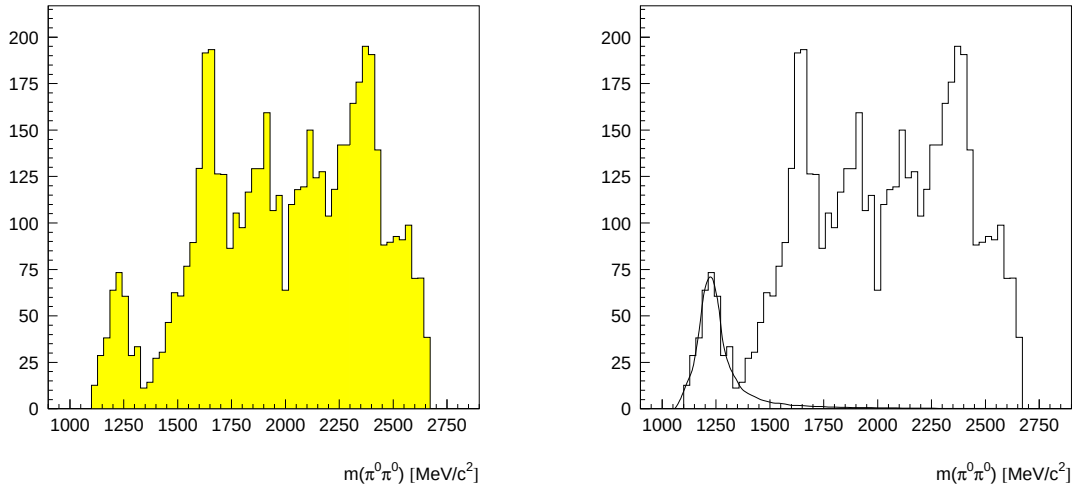

Figure 7.4: *π^0n-invariant mass with $m_{\pi^0\pi^0} \leq 1000\,MeV$, the structure on the left corresponds to the $\Delta(1232)$, the next two peaks are due to the other two nucleon resonance structures at 1650 MeV and 1910 MeV, the three structures in the left part are due to the diagonal bands in the Dalitzplot.*

In order to determine the number of $\Delta(1232)$+n-events in half of the angular distribution (Figure 7.2) is determined.

For this purpose, one needs a good estimate on the background distribution in the Δ-region.

Figure 7.2 shows that for low $\pi^0\pi^0$-invariant masses or for $\cos(\Theta)$ values greater than 0.5 there are almost no events between the two nucleon resonance structures. This means that there should be no background in the $\Delta(1232)$ region, too. However it is necessary to know the background along the $\Delta(1232)$-band for $\cos(\Theta) \geq 0$.

Figure 7.5 shows the projection of Figure 7.2 on the $\cos(\Theta)$ axis for events with $m_{\pi^0 n}$=1232 $\pm$ 120 MeV.

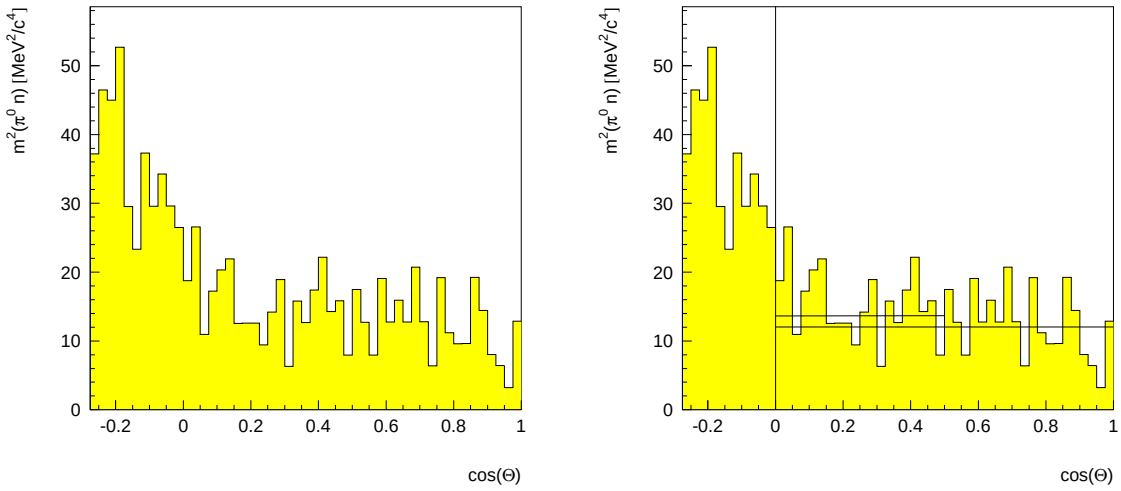

Figure 7.5: $m^2_{\pi^0 n}$-*distribution versus the cos(*Θ*).*

This distribution is, as expected, almost flat with some background contribution at low values of $\cos(\Theta)$. To get an estimate for this background the second half of the $\cos(\Theta)$ distribution (0.5-1) (without the last three bins) was fitted where no background should be and compared to the fit of the first half (0-0.5) (Figure 7.5).We find as background contribution in the region $m_{\pi^0 n}$=1232 $\pm$ 120 MeV:

$$N_{background} = 32 \pm 6 \text{ events} \tag{7.3}$$

The $m_{\pi^0 n}$-distributions in Figure 7.6, with different cuts in $\cos(\Theta)$, were fitted with fixed mass and width of the $\Delta(1232)$ as determined before.

The results of these fits are given in table 7.2 and show, very nicely that the result with a cut at $\cos(\Theta)$=0 is twice as big as the result with the cut at 0.5.

To know now how much of the esminated background events (32 events for $\cos(\Theta) \geq 0$) lie inside the fit curve one has to calculate the difference between the total number of events in the $m_{\pi^0\pi^0}$=1232 $\pm$120 MeV region with the fitted number of events in the same region. This is done in table 7.4:

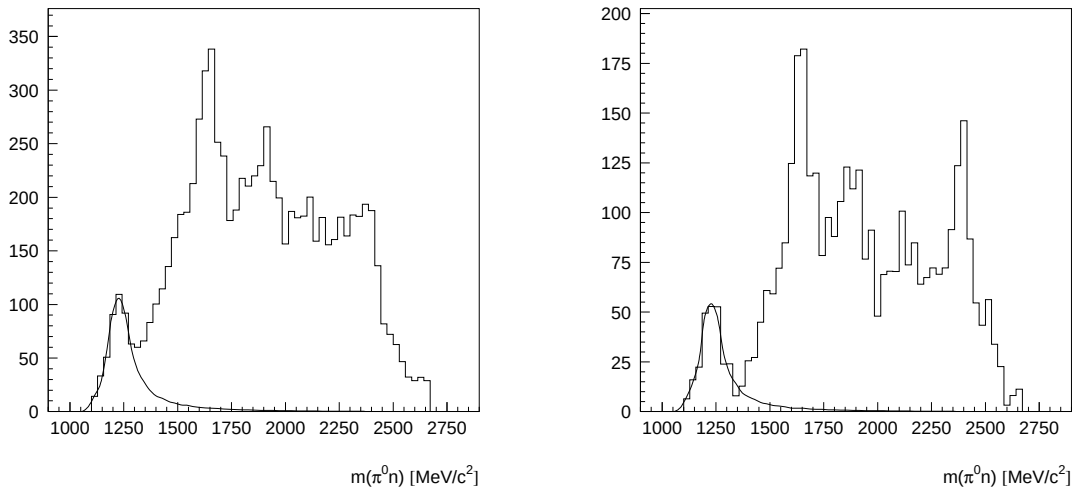

Figure 7.6: *$\pi^0 n$ invariant mass with cos(Θ)≥0 and cos(Θ)≥0.5*

cos(Θ) ≥	no. of events in Breit-Wigner	no. of Breit-Wigner events with m_Δ=1232±120 MeV	no. of events in angular distribution m_Δ=1232±120 MeV (no fit)
0.0	636.4±40.6	513.60	560.66
0.1	566.8±38.3	458.60	487.18
0.2	509.9±36.2	412.97	419.77
0.3	441.0±33.5	357.57	364.64
0.4	391.6±31.7	318.11	312.51
0.5	320.5±28.7	260.59	252.32
0.6	251.6±25.3	203.92	195.12

Table 7.2: *Results of fits for different cuts on cos(Θ), comparison with events in angular distribution (Figure 7.5) with the same cuts.*

cos(Θ) ≥	no. of events in Breit-Wigner	Total no. of Breit-Wigner events -1≤ cos(Θ)≤1 (calculated)
0.0	636.4±40.6	1272.7±81.2
0.1	566.8±38.3	1259.6±85.1
0.2	509.9±36.2	1274.8±90.4
0.3	441.0±33.5	1260.0±95.8
0.4	391.6±31.7	1305.3±105.5
0.5	320.5±28.7	1281.9±114.7
0.6	251.6±25.3	1257.8±126.4

Table 7.3: *Results of fits for different cuts on cos(Θ).*

cos(Θ) ≥	no. of Breit-Wigner events with m_Δ=1232±120 MeV	no. of events in angular distribution m_Δ=1232±120 MeV (no fit)	difference
0.0	513.60	560.66	47.06
0.1	458.60	487.18	28.59
0.2	412.97	419.77	6.8
0.3	357.57	364.64	7.07
0.4	318.11	312.51	-5.6
0.5	260.59	252.32	-8.2
0.6	203.92	195.12	-8.8

Table 7.4: *Comparison of the fit-results with the number of events with m_Δ=1232±120 MeV*

In the cases where we should have no background from $f_2(1270)$ the number of Breit-Wigner-events with m_Δ=1232±120 MeV is a bit higher than the number of events counted (without fit). In the cases where we should have a contribution from the $f_2(1270)$ the sign is opposite and bigger than the estimated background contribution.

If one compares the calculated difference with the estimated background contribution for $\cos(\Theta)\geq 0$ and for $\cos(\Theta)\geq 0.5$ one gets in the first case 15 events less and in the second case 8 events more in the fit than expected. So these considerations lead to an additional error of ±16 events. Notice that one has to multiply the 8 events by two in order to get the error for 1/2 and not only for 1/4 of the angular distribution.

The number of Δ-events was determined to be

$$N^{1/2}_{\Delta(1232)} = 636.4 \pm 40.6\text{events} \tag{7.4}$$

in half of the angular distribution

This result has to be multiplied by two to get the whole number of events

$$N_{\Delta(1232)} = 1277.34 \pm 55.45\text{events} \tag{7.5}$$

Up to this point the dataset was only corrected on the neutron detection efficiency (ε), where the neutron causes only one PED in the barrel. It is also possible that the neutron produces more than one PED. As the best estimate of the probability for the neutron not being detected ε_0 =1-ε-0.02 was used to determine the $\Delta(1232)\pi^0$ branching ratio. A standard deviation $\Delta\varepsilon_0$=0.04 represents a conservative estimate of the combined statistical and systematic uncertainities of the efficiency [1]. So we get a number of

$$N_{\Delta(1232)} = 1314.4 \pm 121.5\text{events}, \tag{7.6}$$

where the error includes the statistical error, the error from the neutron detection efficiency and the error we have calculated before.

The branching ratio for the reaction is derived from the relation:

$$BR = \frac{N_{events}}{\varepsilon_{MC} \cdot BR_d \cdot N_{an}} \ . \tag{7.7}$$

N_{events} is the number of events assigned to the reaction; ε_{MC} the efficiency to detect the 4 photons and to reconstruct the two mesons in the direction of π^0-backward emission ($\cos(\Theta)\geq 0$); BR_d is the product decay branching ratio of the $\pi^0\to\gamma\gamma$ and $\Delta\to N\pi$ (0.994) multiplied by the Clebsch- Gordan coefficient (2/3). With these numbers the final branching ratio is obtained as follows:

$$BR(\bar{\text{p}}\text{d}\to\Delta(1232)\pi^0) = (2.21 \pm 0.24) \cdot 10^{-5} \tag{7.8}$$

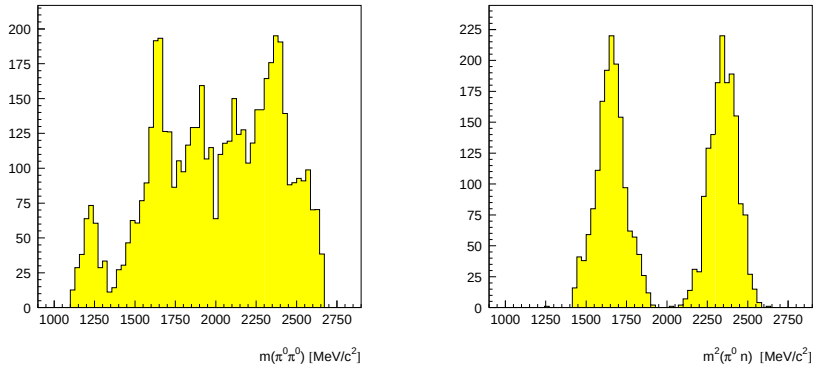

Figure 7.7: *π^0n-invariant mass with $m_{\pi^0\pi^0} \leq 1000\,MeV$: data, Monte-Carlo-simulation of N(1650),f_2(1270)-MC*

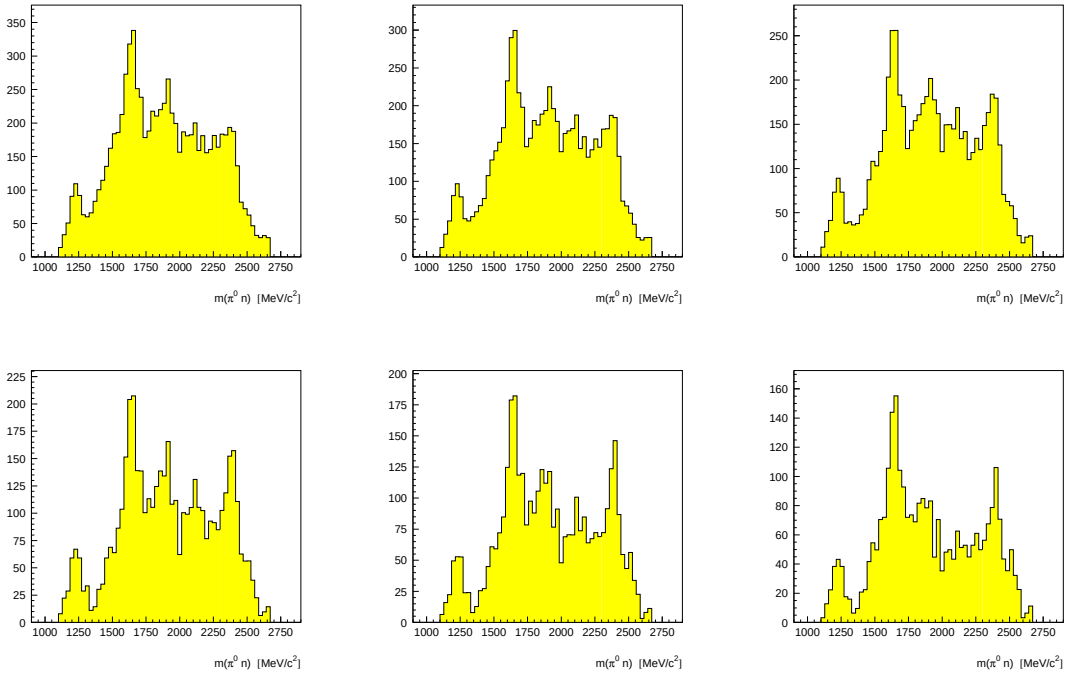

Figure 7.8: *π^0n invariant mass for different cuts in cos(Θ): cos(Θ)≥ 0, 0.1, 0.2, 0.4, 0.5, 0.6*

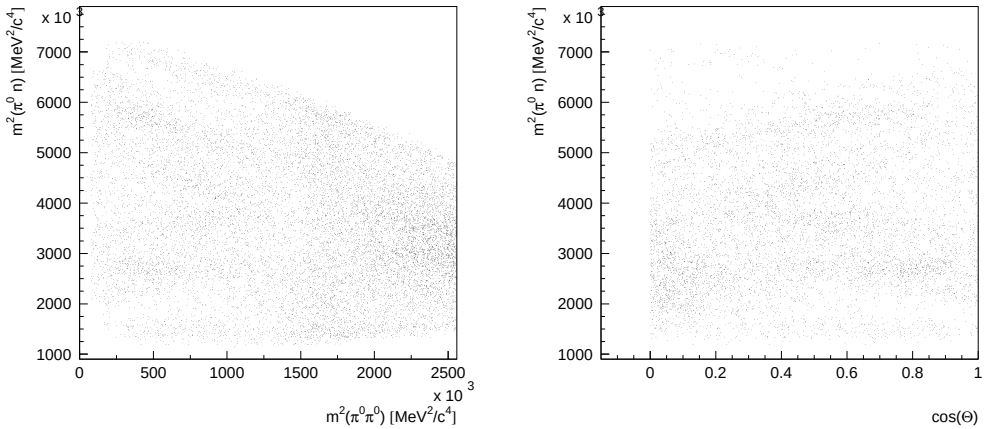

Figure 7.9: *Corrected Dalitzplot and distribution versus the cos(Θ).*

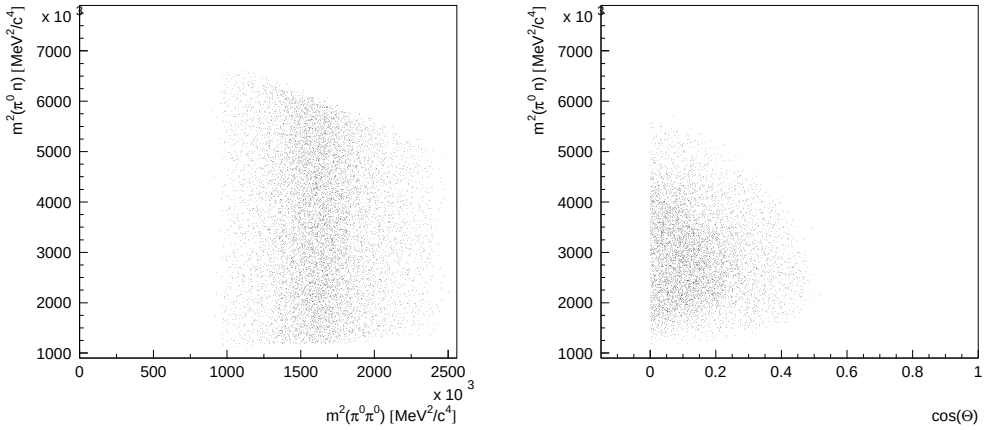

Figure 7.10: *Dalitzplot and distribution versus the cos(Θ): $f_2(1270)$.*

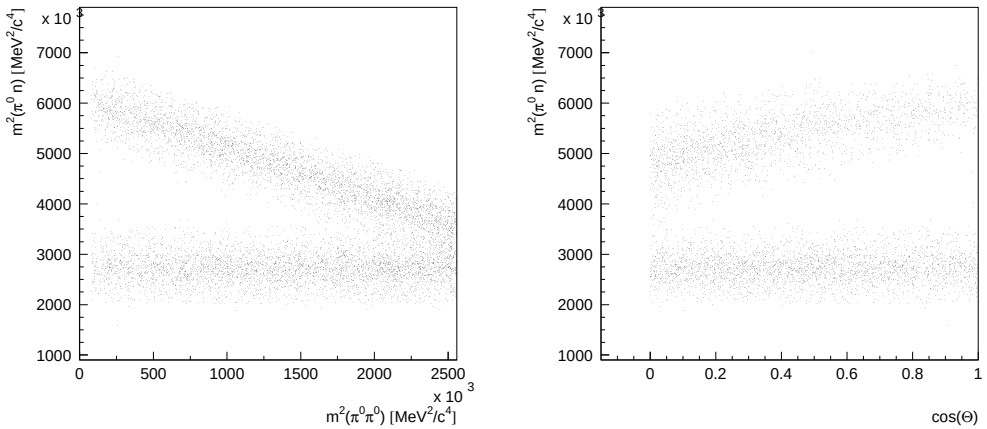

Figure 7.11: *Dalitzplot and distribution versus the cos(Θ): N(1650).*

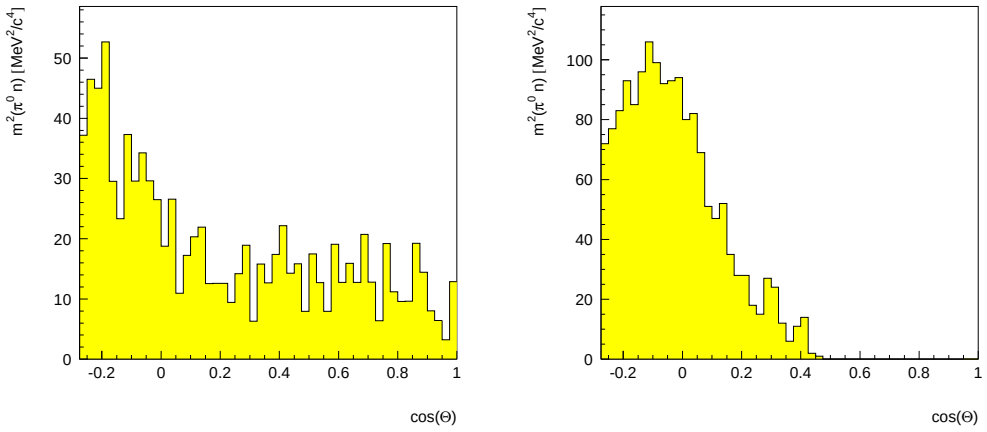

Figure 7.12: *Projektion on cos(Θ) with* $m_{\pi^0 n}$*=1232 ± 120 MeV: data,* $f_2(1270)$

Bibliography

[1] C. Amsler et al. (Crystal Barrel Collaboration), accepted for publication in Zeit. Phys. A (1994)

[2] PhD thesis, Erich Schaefer, Mainz 1993

[3] Review of Particle Properties: L. Montanet et al. Phys. Rev. **D50** (1994)1198